

Dipolar magnetospheres and their characterization as a function of magnetic moment

N. Omidi ^{a,*}, X. Blanco-Cano ^b, C.T. Russell ^c, H. Karimabadi ^a

^a *University of California San Diego, MC 0407, La Jolla, CA 92093, USA*

^b *Instituto de Geofísica, UNAM, Coyoacán D.F., 04510, Mexico*

^c *University of California Los Angeles, P.O. Box 951567, Los Angeles, CA 92093, USA*

Received 6 December 2002; received in revised form 12 December 2002; accepted 10 August 2003

Abstract

Results of two-dimensional (2-D), hybrid (fluid electrons, kinetic ions) simulations of solar wind interaction with a magnetic dipole are presented. This interaction leads to a number of distinct magnetospheres, as the strength of the dipole changes. Both the size and level of complexity of these magnetospheres increases with the dipole moment. A physical parameter which helps characterize these magnetospheres is D_p , the distance ahead of the dipole where the magnetic field pressure balances the solar wind ram pressure. Expressed in units of ion skin depth, when $D_p \sim 0.05$ the interaction results in the formation of a phase standing whistler wake with no change in solar wind velocity or density. When $D_p \sim 0.15$, two additional wakes corresponding to the fast and slow magnetosonic modes are also generated. These two wakes are associated with the formation of a plasma tail, however, no appreciable pile up is observed upstream of the dipole. As D_p approaches 1, a region of plasma pile up is formed resulting in the formation of a fast magnetosonic bow wave standing upstream of the dipole. At the same time, a slow magnetosonic wake is present in the tail region which separates a slower, cooler plasma from a faster and hotter one in the central tail region. Results of test particle calculations suggest that ion acceleration near the dipole is the main source of this plasma. Finally, when $D_p \sim 20$ the resulting magnetosphere has many characteristics similar to those of the Earth and other magnetized planets.

© 2004 COSPAR. Published by Elsevier Ltd. All rights reserved.

Keywords: Dipolar magnetospheres; Solar wind; Magnetic moment

1. Introduction

As the most accessible magnetosphere to mankind, the geospace is also the most studied of all. That the smaller magnetosphere of Mercury (see e.g. Slavin, 2003) and the much bigger magnetospheres of Jupiter or Saturn (see e.g. Russell, 2003) have considerable similarities to that of the Earth's have undoubtedly left the impression that perhaps all dipolar magnetospheres exhibit the same basic properties and overall structure. In investigating the nature of the interaction between the solar wind and magnetized asteroids, Greenstadt (1971) presented a number of conditions that had to be satisfied in order for the resulting magnetosphere to be earthlike. These conditions guaranteed that the gyro-radii of the

solar wind ions is smaller than the distance of the magnetopause from the surface of the asteroid, as well as, the lateral extent of the magnetopause. He also suggested that in the absence of an earthlike magnetosphere the asteroid may have a standing whistler wake. This wake has been further studied by Gurnett (1995), Wang and Kivelson (1996) and Baumgartel et al. (1997) using a variety of approaches and its presence at asteroids Gaspra and Ida has been inferred by (Kivelson et al., 1993, 1995). Recently, Omidi et al. (2002) used two-dimensional (2-D), hybrid (fluid electrons, kinetic ions) simulations of solar wind interaction with magnetic dipoles of various strength in order to investigate the general characteristics of the interaction. The results of this study showed that a number of distinct interactions are possible depending on the strength of the dipole and the distance, D_p at which solar wind ram pressure is balanced by the magnetic pressure of the

* Corresponding author. Tel.: +1-854-534-7304.
E-mail address: nomidi@ece.uscd.edu (N. Omidi).

dipole. Blanco-Cano et al. (2003) compared these simulations with Galileo observations at Gaspra and Ida and found that neither the polarization of the suspected wake nor the inferred size of the interaction region, at these asteroids, is consistent with the simulation results. It was, therefore, concluded that neither asteroid was sufficiently magnetized to result in the formation of a whistler wake. This conclusion is also supported by the recent analysis of magnetic properties of stony (ordinary chondrites) meteorites (Rochette et al., 2003).

In this paper, we summarize the pertinent points of Omidi et al. (2002) and then present aspects of the interaction not discussed before. We also demonstrate that when $D_p \sim 20$ ion skin depth the resulting magnetosphere is earthlike and exhibits similar characteristics, even though $D_p \sim 640$ for Earth. This result establishes the minimum size of an earthlike magnetosphere and explains why magnetospheres as different in size as that of Mercury and Jupiter have similar characteristics.

2. Model

The hybrid simulation model utilized in this study is illustrated in Fig. 1. The size of the simulation domain in each direction, varies between 40 and 600 ion inertial length in order to accommodate for the increasing size of the magnetosphere with stronger dipole fields. Uniform cells with dimensions varying between 0.1 and 1 ion skin depth and containing 10 initial particles are utilized. A line dipole (see Ogino, 1993) is placed at the center of the box with its axis along the Y direction. The cell containing the dipole forms an absorbing region in that all plasma entering this cell is lost. Test runs with no dipole field show that plasma absorption does not lead to any interactions with the solar wind. Initially, the dipole is immersed in a uniform solar wind type plasma which is continuously replenished from the $X = 0$ boundary. In this study, we assign values of 0.5 to electron and ion β (ratio of kinetic to magnetic pressure) for the solar wind with Alfvénic Mach numbers between 5 and 8. The ratio of ion plasma to gy-

rofrequency (the same as the ratio of speed of light to Alfvén velocity) is taken to be 6000. This plasma is allowed to leave the system from the other three simulation walls. Similarly, floating boundary conditions for the electromagnetic fields are applied to these boundaries so that waves can leave the system. While various directions of the interplanetary magnetic field (IMF) have been considered, for the sake of brevity the results presented here all correspond to IMF lying in the X - Y plane and along the Y -axis (i.e., northward IMF condition). In these simulations, the dipole strength was varied by more than five orders of magnitude or $0.05 \leq D_p \leq 21$ ion skin depth. One of the difficulties involved in performing such simulations is the large spatial gradients of the magnetic field which in turn results in variations of ion gyrofrequency and the Alfvén speed. In order to resolve all scales of relevance in the simulations and, at the same time, optimize the computation time the box is divided into two separate zones where both ion motion and electromagnetic fields are solved for using different time steps. Typically time steps of $0.0025 \Omega^{-1}$ (inverse ion gyrofrequency) are used in zone-1 and smaller time steps (by varying factors) are used in zone-2. Finally, a uniform resistivity corresponding to resistive length scale of 0.03 ion skin depth is used. Simulations have been run long enough to achieve a semi-steady state solution. Except for velocity, which is normalized to Alfvén speed, all other plasma and field parameters are normalized to their corresponding solar wind values.

3. Results and discussion

We present the results of simulations starting with the weakest dipole field, corresponding to $D_p \sim 0.05$, and move up in field strength until $D_p \sim 21$. Test simulation runs have shown that when the dipole moment is zero or very small (i.e., $D_p \ll 0.05$) no interaction occurs on ion time or spatial scales. This is consistent with NEAR-Shoemaker magnetic field observations at asteroid 433 Eros which, after a soft landing, established surface field strengths below 1 nT (Acuna et al., 2002). Panel (a) in Fig. 2 shows the log of magnetic field as a function of X and Y at the end of the run with $D_p \sim 0.05$. The interaction results in the formation of a wake which was identified to be in the whistler mode by Omidi et al. (2002). Panel (b) in Fig. 2 shows the x - and z -components of the magnetic field and density along the trajectory “C” in panel (a). The oscillations seen in B_x and B_z are consistent with circular polarization expected from the whistlers (Blanco-Cano et al., 2003). Also, as expected no oscillations in density are observed in association with this wake. In effect, at this level of magnetization the interaction does not affect the solar wind in any appreciable way.

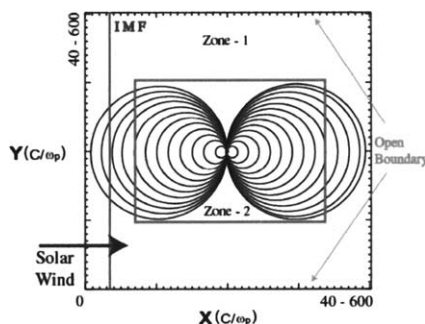


Fig. 1. Illustration of the simulation model used in this study.

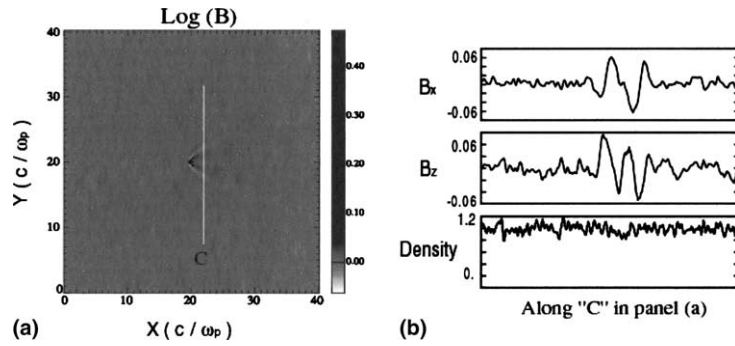


Fig. 2. Panel (a) shows the log of total magnetic field as a function of X and Y at the end of the $D_p = 0.05$ run. Panel (b) shows the variations of x - and z -components of the magnetic field and density along the trajectory “C” shown in panel (a).

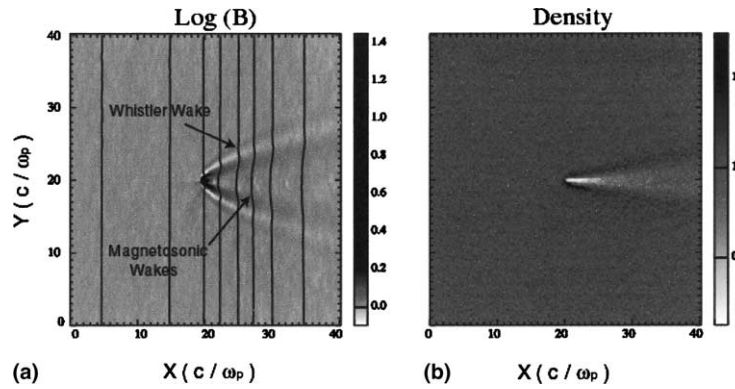


Fig. 3. Log of total magnetic field and density as a function of X and Y are shown in panels (a) and (b), respectively. Panel (a) also shows the magnetic field lines. This simulation corresponds to $D_p = 0.17$ where whistler as well as fast and slow magnetosonic wakes are generated.

Panels (a) and (b) in Fig. 3 show the log of magnetic field and density, respectively, for the case of $D_p \sim 0.17$. The presence of wakes is clear in both panels, however, the cone angle of the magnetic wake is larger than that of the density wake. In other words, magnetic disturbances extend further upstream as compared to the density. It was established by Omidi et al. (2002) that in this case whistler, as well as, fast and slow magnetosonic wakes are formed with the former standing further upstream due to its larger phase velocity. Because of its non-compressive nature, the whistler wake is not associated with density variations as discussed earlier. The fast and slow magnetosonic wakes, on the other hand, are associated with the enhancement of density ($\sim 20\%$) at the edge of the plasma tail. Further into the tail, the density drop associated with the observed cavity is as large as 50%. Due to its propagation characteristics, the whistler wake is confined to planes close to the X - Y plane (e.g. Gurnett, 1995). On the other hand, the magnetosonic modes can propagate in all planes and, therefore, the plasma tail is expected to be much more symmetric with respect to X -axis and to form a true cone.

Despite the formation of a plasma tail, this interaction is not strong enough for solar wind to reach a stage of stagnation in front of the dipole. This is illustrated in

Fig. 4 which shows the variation of density, flow velocity and total magnetic field along a trajectory intersecting the nose of the wake. Here, density and total magnetic field are normalized to their corresponding upstream values while velocity is relative to Alfvén speed. It is clear from this figure that a slight enhancement in density and reduction in flow speed occurs just upstream of the dipole center (i.e., where peak B is observed). Due to the small value of D_p in this case, the point of stagnation is too close to the dipole for the plasma to pile up. Essentially, the fast and slow magnetosonic wakes accommodate the necessary flow diversion around the magnetic obstacle in this case.

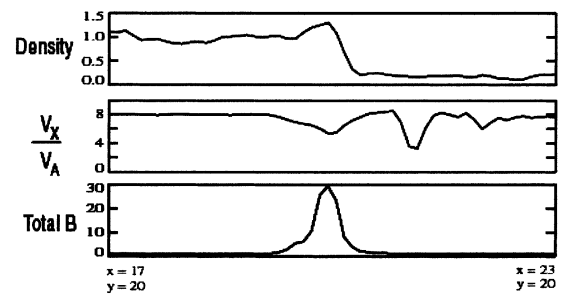


Fig. 4. Variation of density, flow velocity and magnetic field along a trajectory through the subsolar point for the $D_p = 0.17$.

Increasing the dipole strength so that $D_p \geq 1$, results in a new type of interaction. Specifically, plasma stagnation occurs upstream of the dipole and a fast magnetosonic bow wave forms which diverts the flow around the obstacle. An example of this type of interaction is illustrated in Fig. 5 which corresponds to $D_p \sim 2.2$. Note that the simulation box is larger than the previous runs due to the increase in the size of the resulting magnetosphere. As expected for the fast magnetosonic mode, the bow wave is associated with increase in density and magnetic field strength upstream of the dipole. Despite similarities to a fast shock, the spatial scales associated with the bow wave are comparable to the ion gyroradii and therefore different dissipation processes are at work. For example, it was shown by Omidi et al. (2002) that ion reflection by the bow wave and the subsequent $E \times B$ acceleration of these ions leads to global asymmetries in the wave structure. Formation of a stagnation point/region near $X \sim Y \sim 100$ is clear in Fig. 5 which shows enhancement of density in this region. As expected, this stagnation point forms ~ 2 ion skin depths upstream of the dipole. Piling up of magnetic field lines, downstream of the fast wake, is also evident in Fig. 5. Due to the geometry of the dipole and IMF fields, two null points are formed in the high latitude region. Although similar to a reconnection process, the size of the null region is smaller or comparable to ion gyro-scales and therefore, would correspond to an unmagnetized ion regime of magnetic reconnection. Reconnected magnetic field lines are evident in Fig. 5. Also, a region of lower magnetic field strength is present within the central part of the tail. The boundary of this region flares out with distance away from the dipole and is closely aligned with changes in the magnetic field direction. We identify this boundary as a slow mode wake and explore its properties in some detail.

Examination of the plasma properties in the tail region shows the presence of two distinct population of

ions. One corresponds to a heated and decelerated solar wind which flows around the obstacle. The other is an even hotter population, confined to the central tail, moving away from the dipole with velocity equal to solar wind speed. These two populations can be seen in panel (a) in Fig. 6 which shows the ion temperature as a function of X and Y . The increase in temperature associated with the bow wave is evident. Some of this heated plasma is seen to escape back upstream from the quasi-parallel (top and bottom) portions of the bow wave. Panel (b) in the figure is a blow up of the tail region near the dipole and demonstrates the presence of the hot population of ions on the reconnected field lines. The panel also shows that change in the magnetic field direction is closely aligned with the outer boundary of these ions. To further illustrate the variation of plasma and field properties across the tail, Fig. 7 shows density, temperature, flow velocity along the x -axis and total magnetic field along the trajectory labeled “L” in panel (a) of Fig. 6. The abbreviations “FW” and “SW” correspond to fast bow wave and slow wake, respectively. The trajectory “L” begins upstream of the top side bow wave and ends upstream of the down side bow wave. The presence of backstreaming ions in the solar wind

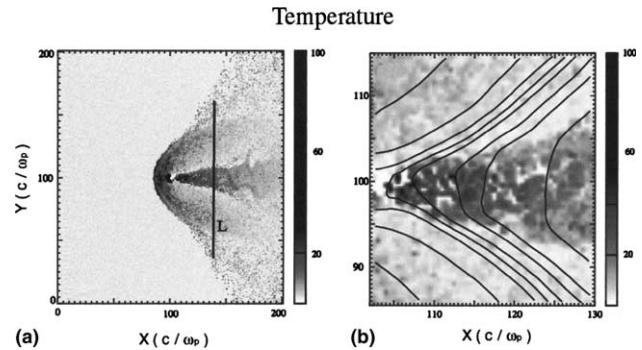


Fig. 6. Panel (a) shows the ion temperature for the $D_p = 2.2$ case. Panel (b) shows the same except in region near and behind the dipole.

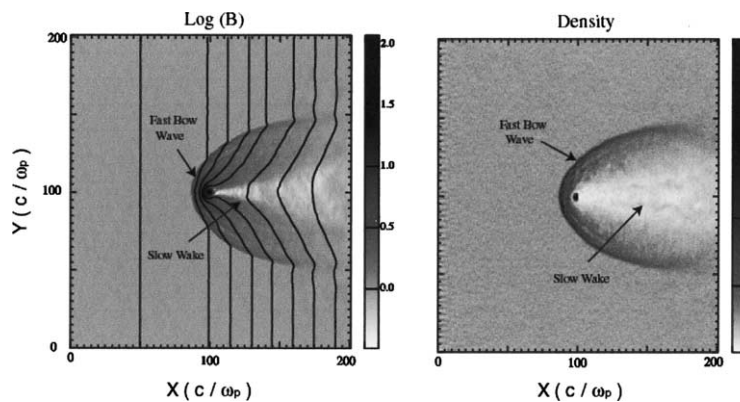


Fig. 5. The same as Fig. 3 except that $D_p = 2.2$. The interaction involves the formation of a fast bow wave, a slow magnetosonic wake and a plasma stagnation region ahead of the dipole.

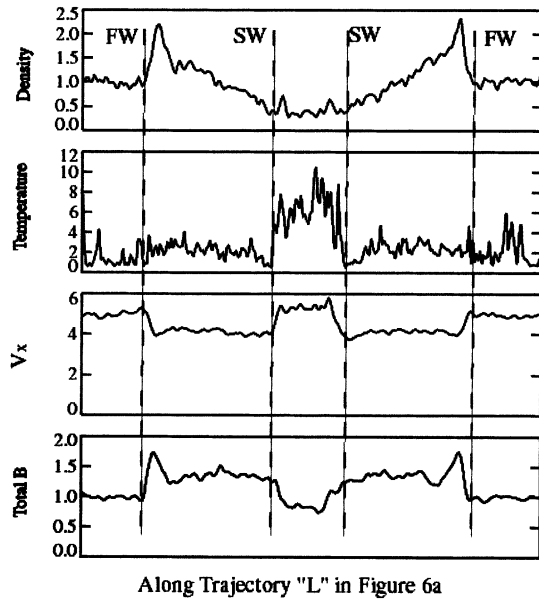


Fig. 7. Variations of density, temperature, flow velocity along x and total magnetic field along the “L” trajectory across the tail. The bow wave “FW”, results in deceleration, compression and heating of the incident solar wind. The slow wake “SW”, bounds a hotter and faster plasma in the central tail.

gives rise to artificial jumps in ion temperature upstream of the bow wave. The change in plasma parameters across this wave is consistent with the expectations for the fast mode. Downstream of the bow wave, the density drops continuously while ion temperature, velocity and magnetic field are essentially constant.

Sharp changes in plasma and field parameters are evident across the slow wake. While the change in plasma density is localized to the wake region the changes in temperature, flow speed and magnetic field extend throughout the central tail. Interpretation of the wake as the slow mode is consistent with the anti-correlation between density and magnetic field. In fact, the drop in magnetic field, along with the increase in

temperature and V_x , across the wake, is similar to signatures associated with slow shocks. It is, therefore, natural to wonder the extent to which the slow wake contributes to the observed heating and acceleration of the ions in the central tail.

To address this question, we have conducted a number of test particle calculations in which ions with velocity and temperature similar to solar wind, were injected in different regions of the simulation box. Using the electromagnetic fields obtained from hybrid simulations at the end of the run, the trajectories of these ions were calculated and compared to the simulation results. Although, ignoring the time dependence of the electromagnetic fields is not completely justified it does provide for a simple and useful tool of analysis. Fig. 8 shows the results of two sets of calculations corresponding to ion injection in different regions of the simulation box. Specifically, in one case (left panel) solar wind type ions were injected upstream of the bow wave in the region $X = 50$ and $25 \leq Y \leq 175$. In the other case (right panel), solar wind type ions were injected near and behind the dipole i.e., $X = 105$ and $95 \leq Y \leq 105$. The left panel shows heating and diversion of the ions at the bow wave. In addition, leakage of ions into the upstream regions of the quasi-parallel sides of the bow wave are reproduced very well in the test particle calculations. In general, a comparison with panel (a) in Fig. 6 shows that the injection of ions upstream of the bow wave results in a temperature profile similar to that in the simulation except for the absence of the central tail population. On the other hand, injecting ions near the dipole results in a pattern of accelerated ions which resembles the profile of the central tail population (right panel). We have also, performed test particle calculations in which ions are injected further downstream of the dipole so that acceleration by the slow wake alone could be investigated. The results show little sign of ion energization by the wake. Based on these results, we conclude that although the slow wake may contribute to heating of the ions in

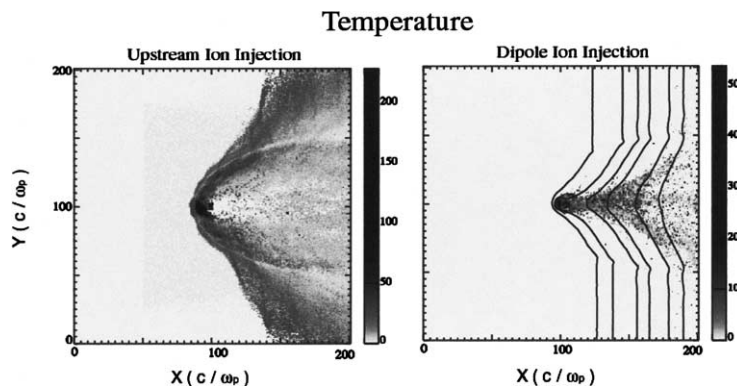


Fig. 8. Results of test particle calculations for two cases of ion injection in the upstream (left panel) and dipolar regions (right panel). The results suggest that the bow wave results in the heating and diversion of the solar wind ions, while ion acceleration by the magnetic dipole accounts for the hot, fast plasma in the central tail.

the central tail region, the bulk of acceleration and heating takes place near and inside the dipolar field region. It is interesting to note (see right panel in Fig. 8) that even though ions were injected behind the dipole, the dayside of the dipole is also populated by the energetic ions. This is partially possible due to the interconnection of the field lines but also to finite gyro-radii effects.

To summarize the $D_p = 2.2$ case, the interaction results in the formation of fast bow wave and a slow magnetosonic wake. The bow wave results in the deceleration, heating and diversion of the incident solar wind ions. The slow wake, in the tail, bounds a hotter and faster plasma population. Ion acceleration near and within the dipole region accounts mostly, if not completely, for the presence of this plasma. Although, the slow wake may not be a major contributor to ion acceleration it does influence the propagation characteristics of the accelerated ions. A more detailed discussion on the nature of the acceleration process by the dipole field will be presented elsewhere.

Increasing the dipole strength beyond $D_p = 2.2$ gives rise to incremental changes in the structure of the resulting magnetosphere. These changes are towards an earthlike magnetosphere and first occur in the dayside. Specifically, the decreasing size of the ion gyro-radii relative to the dipolar field region gives rise to a boundary which resembles the dayside magnetopause at the planets. In effect, separation of plasma into two distinct populations of solar wind and magnetospheric is possible when the ion gyro-radii becomes much smaller than the size of the magnetopause boundary. The tail region of the magnetospheres are found to be quite dynamic as D_p increases, and show an initial earthlike structure before settling on solutions similar to smaller D_p cases. By the time $D_p \sim 20$ however, the resulting magnetosphere has many earthlike characteristics both in the dayside and in the tail. As an example, Fig. 9 shows the log of magnetic field and ion temperature

from a run corresponding to $D_p = 21$. Formation of a fast bow shock, magnetosheath, magnetopause, cusps and a central plasma sheet bounded by boundary layers is among the characteristics found in this run.

It is evident from Fig. 9 that magnetic reconnection plays an important role, in the dynamics of this magnetosphere, by the formation of plasmoids in the high latitude magnetopause and the central tail region. The fact that the plasmoids at the magnetopause are at high latitudes is consistent with the northward direction of IMF and time dependent reconnection near and on the tail side of the cusps. These plasmoids propagate towards the tail and may coalesce into bigger magnetic islands, as can be seen in the bottom flanks of the magnetopause. Magnetic reconnection in the central tail region is associated with the thinning and the unstable nature of the current sheet associated with the stretching of the tail field lines. This process gives rise to a fairly time stationary neutral point with dipolar fields on one side and highly stretched and reconnected fields on the other.

The presence of energetic ions, resulting from this interaction, is evident in the dipolar, magnetopause and central tail regions. Assuming a solar wind ion temperature of 10^5 K, maximum ion energies of ~ 40 keV are obtained. Examination of the spatial distribution of the accelerated ions shows the most energetic to be, generally, confined to the dipolar region. Although, the distribution of energetic ions in the high latitude magnetopause and the central tail region is by no means uniform, most have ~ 1 keV energies. With regard to sources and regions of acceleration a number of possibilities are evident. Specifically, ion acceleration by the dipole, as well as, magnetic reconnection are most likely involved. The spatial distribution of the energetic ions suggests that dipole acceleration generates the most energetic particles and accounts for the majority of the ions in the dipolar region. It is also expected that this process contributes to the energetic ions in the magnetopause and the central tail regions.

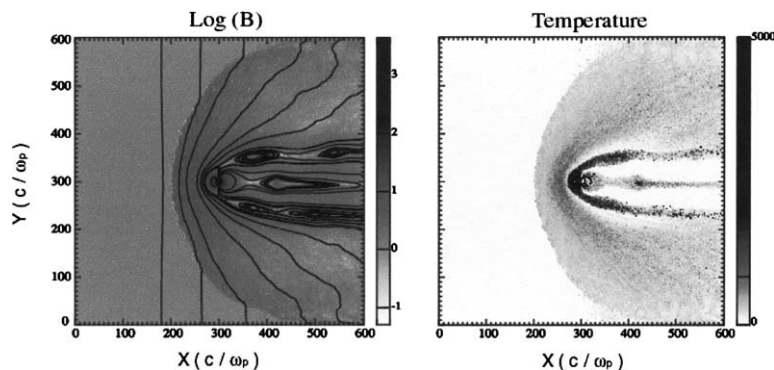


Fig. 9. Log of total magnetic field and temperature for the case $D_p = 21$ which has a terrestrial type magnetosphere. The magnetic field lines show the formation of plasmoids in the high latitude magnetopause and the central tail region. Ion energization in these as well as the dipolar regions is evident with maximum energies reaching 40 keV.

Presence of energetic ions in the plasmoids, however, is also an indication that magnetic reconnection contributes to ion acceleration in the magnetopause and tail. Clearly, generation of energetic particles observed in this run is quite significant and could have ramifications regarding the formation of radiation belts and observations of high energy ions in the magnetopause and tail regions of planetary magnetosphere. More details regarding these acceleration processes will be presented elsewhere.

The fact that an earthlike magnetosphere is formed when $D_p \sim 20$ has a number of implications which we briefly discuss now. With regard to the topic of comparative magnetospheres, this result demonstrates why a terrestrial-type magnetosphere has been associated with planets as diverse in size as Mercury and Jupiter (see e.g. Slavin, 2003; Russell, 2003). Given that $D_p \lesssim 75$ for these planets, one would expect them to have magnetospheres that are earthlike in their overall structure. Of course, the self-similar/terrestrial-type nature of the magnetospheric solutions for $D_p \sim 20$ and larger does not imply that all magnetospheric processes at planets are similar. For one thing, variations in the planetary radii or the presence or absence of ionospheres or moons make each magnetosphere unique. Further, variations of the overall size of the system with D_p could, by itself, cause inherent differences in the behavior of the magnetosphere. For example, in the case of the Hermean magnetosphere it has been argued, by Luhmann *et al.* (1998), that since it takes a parcel of solar wind about 1 min to traverse the length of the magnetosphere, the system is more “driven” and responsive to solar wind changes. In addition, it is possible that a given physical process may be associated with spatial scales that are too large to fit some earthlike magnetospheres and therefore, absent from them while operative in bigger magnetospheres. Despite these points, however, it is clear that much can be learned about the basic properties of terrestrial type magnetospheres and the underlying physical processes using smaller size magnetospheres. This is particularly important for kinetic global simulations in that although current computational limitations make it hard to simulate earth-sized magnetospheres in three-dimensional (3-D), it is still possible to apply these simulations to magnetospheric physics.

4. Concluding remarks

We have used the results of 2-D hybrid simulations to characterize the nature of solar wind interaction with a magnetic dipole and demonstrate that a variety of interactions, ranging from a simple whistler wake to an earthlike magnetosphere, are possible. For the sake of brevity, we have only considered the cases with purely northward IMF and as a result, have skipped over many interesting and important issues related to intermediate

or southward IMF geometries. Similarly, we have only considered a single orientation for the dipole axis and have ignored effects associated with having a component of the flow velocity along the dipole axis. These, plus many other effects remain to be investigated in the future using the ion kinetic approach. It is clear, from the results presented here, that hybrid simulations are capable of addressing many critical problems in magnetospheric physics in ways not previously possible. That smaller magnetospheres can be used to investigate the nature of the planetary magnetospheres, opens the doors to 3-D global hybrid studies of magnetospheric physics. Of course, much more remains to be learned from 2-D global simulations as well. These simulations are not only useful due to their less computational needs, but also the ability to eliminate various physical processes from a given simulation run as part of data analysis and interpretation procedure (see e.g. Omid *et al.*, 2002). Finally, application of these results to asteroids suggests that a wide variety of asteroidal magnetospheres may exist depending on their intrinsic, global field strength. Determination of magnetic properties of asteroids is an important component of understanding of their origin and whether they are part of a larger, differentiated parent body. This, plus the possibility of observing and investigating new types of magnetospheres introduce strong incentives for future missions to asteroids with proper plasma and field instruments.

Acknowledgements

The work at UCSD was performed under the auspices of the California Space Institute and was supported by NASA Grants NAG5-9314, NAG5-11754, and NSF grant ATM-0119846. The use of multiple-time-grid hybrid code developed by SciberNet Inc. is acknowledged.

References

- Acuna, M.H., Wasilewski, P., Kletetshka, G., *et al.* NEAR magnetic field observations at 433 Eros: first measurements from the surface of an asteroid. *Icarus* 155, 220–228, 2002.
- Baumgartel, K., Sauer, K., Story, T.R., *et al.* Solar wind response to a magnetized asteroid: linear theory. *Icarus* 129, 94–105, 1997.
- Blanco-Cano, X., Omid, N., Russell, C.T., *et al.* Hybrid simulations of solar wind interaction with magnetized asteroids: comparison with Galileo observations near Gaspra and Ida. *J. Geophys. Res.* 108, 1–13, 2003.
- Greenstadt, W. Conditions for magnetic interaction of asteroids with the solar wind. *Icarus* 14, 374–381, 1971.
- Gurnett, D.A. The whistler-mode bow wave of an asteroid. *J. Geophys. Res.* 100, 21,623–21,629, 1995.

- Kivelson, M.G., Bargatze, L.F., Khurana, K.K., et al. Magnetic field signatures near Galileo's closest approach to Gaspra. *Science* 261, 331–334, 1993.
- Kivelson, M.G., Wang, Z., Joy, S., et al. Solar wind interaction with small bodies, 2. What can Galileo's detection of magnetic rotations tell us about Gaspra and Ida. *Adv. Space Sci.* 16 (4), 47–57, 1995.
- Luhmann, J.G., Russell, C.T., Tsyganenko, N.A. Disturbances in Mercury's magnetosphere: are the Mariner 10 "substorms" simply driven? *J. Geophys. Res.* 103, 9113–9119, 1998.
- Ogino, T. Two-dimensional MHD code, in: Matsumoto, H., Omura, Y. (Eds.), *Computer Space Plasma Physics: Simulations and Software*. Terra Scientific Publishing, Tokyo, pp. 161–191, 1993.
- Omid, N., Blanco-Cano, X., Russell, C.T., et al. Hybrid simulations of solar wind interaction with magnetized asteroids: general characteristics. *J. Geophys. Res.* 107, 1–10, 2002.
- Rochette, P., Sagnotti, L., Bourt-Denise, M., Consolmagno, G., Folco, L., Osete, M., Pesonen, L. Magnetic classification of stony meteorites: 1. Ordinary chondrites. *Meteoritics and Planetary Sciences* 38 (2), 251–268, 2003.
- Russell, C.T. Outer planet magnetospheres: a tutorial. *Adv. Space Res.*, 2004, this issue, doi:10.1016/j.asr.2003.04.049.
- Slavin, J.A. Mercury's magnetosphere. *Adv. Space Res.*, 2004, this issue, doi:10.1016/j.asr.2003.02.019.
- Wang, Z., Kivelson, M.G. Asteroidal interaction with the solar wind. *J. Geophys. Res.* 101, 24,479–24,493, 1996.